Intrusive origin of a 4.8-meter-thick ground ice body within a polygonal peatland along the Inuvik-Tuktoyaktuk Highway, NWT

Alejandro Alvarez[1], Jordan Harvey[1], Alexandre Chiasson[1], Joseph M. Young[1], Steven V. Kokelj[2], Peter D. Morse[3] & Duane Froese[1]

[1]*PACS Lab, Department of Earth and Atmospheric Science, University of Alberta, Edmonton, Canada*

[2]*Northwest Territories Geological Survey, Government of the Northwest Territories, Yellowknife, Canada*

[3]*Geological Survey of Canada, Natural Resources Canada, Ottawa, Canada*

Abstract

A seemingly unusual 4.8-m-thick ground ice body between 2.1 m and 6.9 m depth, within a polygonal peatland adjacent to the Inuvik-Tuktoyaktuk Highway (ITH), was recovered by the Sentinel drill program in 2017. Characterizing the nature of large ground ice bodies is necessary for predicting the potential effects of ground ice thaw on highway embankment stability. Here, we characterize the ground ice body and hosting sediments using Computed Tomography (CT), radiocarbon dating, geochemistry (δD, δ^{18}O, and d-excess), and cryostratigraphy. CT scanning was performed to quantify ice textures, including bubble content, shape, size, and orientation. The ice has a milky-white to clear horizontal tabular appearance with consistent vertical bubble train dispersals. Stable isotopes range from -27‰ to -18‰ (δ^{18}O) and -219‰ to -149‰ (δD), comparable to modern isotope values and a co-isotope slope similar to the local meteoric water line. This indicates ice formation likely derived from atmospheric water sources, with little evaporative transformation, in the Late Holocene. Given the thickness, sharp upper contact with the peat, and tabular appearance, we interpret this ground ice body as being of injection ice origin. Injection ice is typically not associated with peatlands, but has been observed in isolated occurrences in the area. The results here indicate that polygonal peatlands, widespread throughout the western Arctic and along the ITH, may have higher ground ice contents and potential for subsidence than previously inferred.

1 Introduction

The Inuvik-Tuktoyaktuk Highway (ITH) traverses ice-rich, continuous permafrost with a wide range of vegetation, surficial geology, and ground ice types. Ice-rich terrain, and in particular large bodies of ground ice, can pose considerable risk to infrastructure due to the terrain implications associated with thaw. Understanding the origin of ground ice types and their associated geomorphic context provides insight into variation in terrain sensitivity and potential hazards associated with permafrost thaw. One common type of ground ice found within the area is injection (or intrusive) ice. Injection ice is formed by the pressurized intrusion of water into soils or rock, uplifting the overlying materials and freezing to form bodies of ice (Mackay 1972). Typical cryostructures of injection ice are described in Pollard (1990) and Mackay (1990), which include layered, suspended, and solid (pure) ice, while typical cryotextures include tubular bubbles, long bubble trains, stratified bubbles and potential inclusion of small bubbles and crystals along chill margins. Injection ice is usually found at shallow depths, within the former active layer (Mackay 1972; Pollard and French 1985); however, injection ice has also been observed deeper within permafrost, whereby water is injected deep along fractures (Mackay 1989). Previous work has described injection ice as a driver of frost blister formation (Pollard and French 1985; Pollard 1990; Morse and Burn 2014), ice dykes (Mackay 1989; Mackay and Dallimore 1992), sill ice (Mackay, 1972), and pingo ice (Mackay, 1990). Here, we characterize a 4.8-m-thick body of ice from a borehole (NTGS 17-01; Figure 1) in a polygonal peatland that does not conform to traditional wedge ice or pool ice structural or geochemical characteristics. Our interpretation of the origin of this ground ice body is based on cryostratigraphy, cryotextures, and isotopic analyses that provide insight into processes of ground ice formation. We propose a conceptual model involving multiple episodes of injection ice forming an unusually thick body of ground ice in a peatland setting.

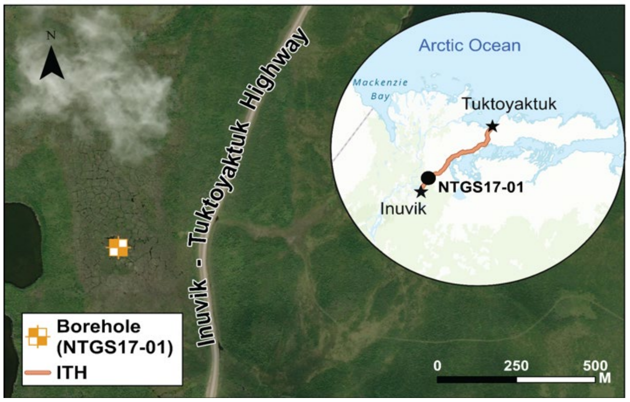

Figure 1. Location of study area. NTGS17-01 is located within a high-centred polygonal peatland west of the ITH.

2 Study Area

The polygonal peatland hosting the 4.8-m-thick ground ice body is located ~20 km north of Inuvik, 260 m west of the ITH, NT, Canada (68.54°N, -133.77°W). This site lies within the continuous permafrost zone and is in tall-shrub tundra within the limits of the northern boreal treeline. The vegetation at this peatland is mainly low shrub (*Salix spp.*)

https://doi.org/10.52381/ICOP2024.232.1

with heath ground cover. The peat deposit overlies hummocky Pleistocene till of the Laurentide Ice Sheet ca. 18,000 to 13,100 ^{14}C years BP (Rampton 1988; Lacelle et al. 2004; Kennedy et al. 2010). The mean annual air temperature in Inuvik is -6 °C (Kokelj et al. 2017) and mean annual ground surface ground temperature (MAGST) and mean annual ground temperature (MAGT) at a depth of 2 m are -0.7 °C and -1.8 °C, respectively (Rudy et al. 2020). The active layer is ~0.8 m thick (Figure 2B). This site is at a polygonal peatland with mainly high-center polygons within an old lake basin. The polygons are predominantly non-orthogonal in shape (120°, Y-junction), with high connectivity of ice-wedge troughs, several of which exhibit active thermokarst degradation and host small trough ponds.

3 METHODS

A collaborative drilling program funded by the Government of Northwest Territories was carried out along the ITH in March 2017 (for details on the program see Ensom et al. 2020). Our study analyzes borehole NTGS17-01, drilled in a polygonal peatland to a depth of 11.2 m. All core samples were sectioned in the field, logged, and transported frozen to the University of Alberta's Permafrost Archives Science (PACS) Lab. In the laboratory, cores were scraped to reveal textures, photographed, and characterized following the cryostructure classification of Murton and French (1994). Subsequently, cores were subsampled at ~20 cm intervals to analyze for water isotopes (δ^{18}O and δD) using a Picarro L2130-i water isotope analyzer. Two reference waters, USGS 45 and USGS 46, were used to calibrate measurements to the Vienna Standard Mean Ocean Water (VSMOW) – Standard Light Antarctic Precipitation (SLAP) scale with internal precisions of ± 0.5‰ and ± 0.1‰ for δD and δ^{18}O. Additionally, some of the core segments were sampled at higher resolution (~2 cm) to sample different cryotextures. One radiocarbon date was determined on a mixed terrestrial plant material sample, pretreated following a standard acid-base-acid preparation (c.f., Reyes et al. 2010) at the university of Alberta, and shipped to the A.E Lalonde AMS Laboratory, University of Ottawa.

Computed tomography (CT) scans were used to determine core characteristics and statistical analysis were done on segmented images to characterize gas inclusions (gas bubbles). The scans were carried out at the PACS lab with a Nikon XTH 225 ST Industrial CT scanner using an insulated container containing dry ice to hold samples below -10ºC. The CT scans used a beam energy of 150 Kv and an exposure time of 8fps, resulting in an effective voxel size of ~60µm. The primary TIFF images were reconstructed into three-dimensional volume files using Nikon CT Pro 3D software and imported into ORS Dragonfly 3D visualization software (ver. 2022.1.0.1249). Representative boxes were selected within each core to avoid edge effects. Within each box, regions of interest (ROIs) were defined for ice and bubbles using Dragonfly's Otsu splitting method, enabling automatic segmentation (c.f., Roustaei et al. 2022). Gas bubble ROIs were further processed using Dragonfly's multi-ROI analyses, where bubble characteristics and statistics, including sphericity (degree of how close a bubble resembles a sphere, where a sphericity of 1 is a perfect sphere), Feret diameter (diameter of longest bubble axis), orientation and volume, were calculated. In some cases, multi-ROIs were refined by removing gas bubbles smaller than 10 voxels to allow for greater visual clarity. CT scan ROIs and water isotopes were sampled in the middle of the core to mitigate any biases from the core sampling method.

4 RESULTS AND ICE CHARACTERISTICS

The NTGS17-01 borehole is distinguished by three main stratigraphic deposits that were subdivided into six units based on differences in cryostratigraphic characteristics (Figure 2A). A peat deposit with a thickness of 2.1 m, overlies a ground ice deposit of 4.8 m (2.1 to 6.9 m depth). The ice body displays a mostly milky white tabular appearance and has a sharp lower contact with an underlying ice-poor diamict. The ice-poor diamict deposit, which extended from 6.9 m to the full depth of the borehole at 11.2 m, is dark grey and matrix-supported with clasts, varying in size between pebbles and cobbles. One radiocarbon date was collected from NTGS17-01 at the upper peat-ice contact, at a depth of 2.0 m (Figure 2A). The water isotope (δ^{18}O and δD) values in the NTGS17-01 borehole have values that are similar to modern precipitation in Inuvik (Fritz et al. 2022). The uppermost peat unit has average δ^{18}O and δD (± standard deviation) values of -18.9 ± 0.8‰ and -152.7 ± 6.2‰, respectively (Figure 2A). The underlying ground ice deposit is more depleted, with average δ^{18}O and δD values of -23.5 ± 3.1‰ and -189.5 ± 22.4‰, respectively, but shows a greater range in values than the underlying diamict or overlying peat deposits. By comparison, the local meteoric water line (LMWL) at Inuvik has a slope of 7.4 (Fritz et al. 2022). In contrast, the regression slope of the ice-poor diamict is lower, at 3.2 (Figure 4). Below we describe six units within the three main deposits (peat, ice and diamict) at this site

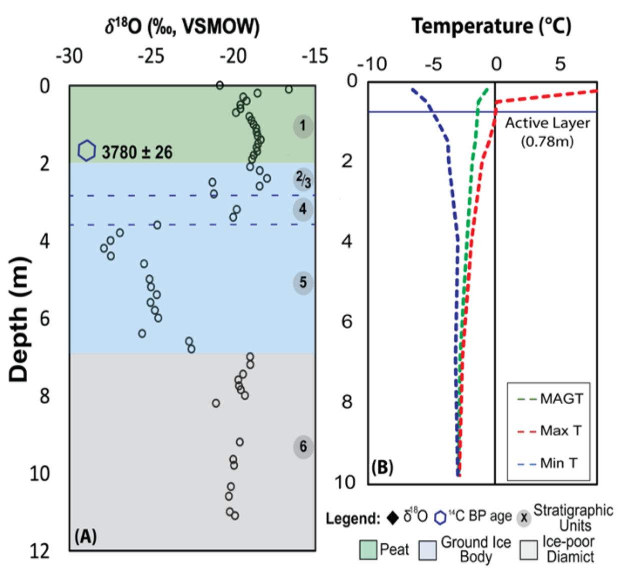

Figure 2. NTGS17-01 summary. (A) δ^{18}O profile, radiocarbon, three stratigraphic deposits (peat, ground ice body, and ice-poor diamict), and the six units. (B) Mean, maximum and minimum annual ground temperatures.

based on variations in cryostructures, and cryotextures, which comprise microscopic textures and features, including bubble shape, orientation, and volume.

4.1 Unit 1: Peat Unit

The peat unit (0 m to 2.1 m) has a dark-brown massive appearance, predominantly composed of organic-matrix and rare crustal cryostructures (Figure 3a). The CT scan statistics show a low concentration of gas bubbles within the peat, with an average of 4%. This value represents the volume of gas bubbles relative to the volume of the sample within an ROI. Gas bubbles within the peat unit have a mean Feret diameter of 0.56 mm, a mean volume of 0.05 mm^3, and a mean sphericity of 0.81. Towards the base of the peat unit, sitting above the basal ice contact, there are tubular bubbles which tend to narrow downwards and have a maximum Feret diameter between 6 and 10 mm (Figure 5A).

4.2 Unit 2: Contact Unit

The contact unit (2.1 to 2.3 m) includes the contact of the ice body and the overlying peat (Figure 3a). The ice portion has a milky-white appearance with layered and suspended cryostructures, including angular organic inclusions (Figure 3a). A radiocarbon date of 3,780 ± 26 (UOC-5201) was obtained at 2.0 m depth, right above the peat–ice contact. A bimodal distribution of bubbles is present at the soil–ice contact, with large downward-tapering bubbles from the overlying peat unit and small bubbles within the ice (Figure 5A). This unit has a high concentration of small gas bubbles, whereby 21% of this unit is composed of gas bubbles, illustrated by the opaque nature of the ice and CT images (Figure 5A). The gas bubbles within the ice have a mean Feret diameter of 0.33 mm, a mean volume of 0.01 mm^3, and a mean sphericity of 0.88. Tubular bubbles with a maximum Feret diameter between 5 and 7 mm are present within the suspended peat inclusions and tend to narrow downwards (Fig. 5a).

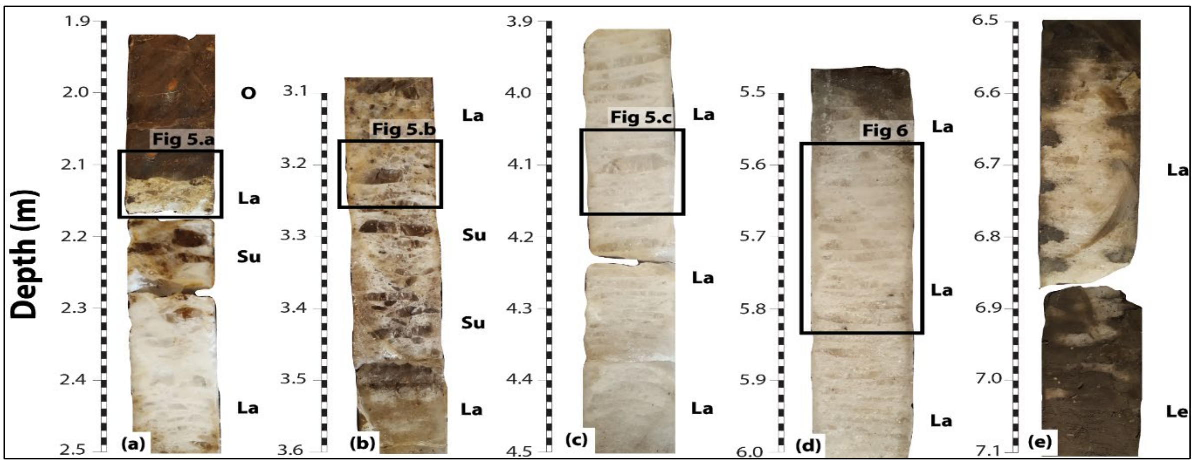

Figure 3. Representative core segments of borehole NTGS17-01 highlighting different cryostratigraphic units and cryostructures. The black boxes represent inset figures of scanned CT images in Figure 5 and 6. (a) Peat unit (0 to 2.1 m), contact unit (2.1 to 2.3 m), and upper layered unit (2.3 to 2.5 m). (b) Brecciated unit (3.1 to 3.5 m). (c–d) Lower layered unit (3.5 to 6.9 m), including location of CT scan in Figure 6. (e) Lower sharp contact between ground ice (unit 5 lower layered unit) and ice-poor diamict unit (6.8 to 11.2 m). Cryostructures shown to the right of the core segments include Layered (La), Suspended (Su), Organic-Matrix (O), and Lenticular (Le).

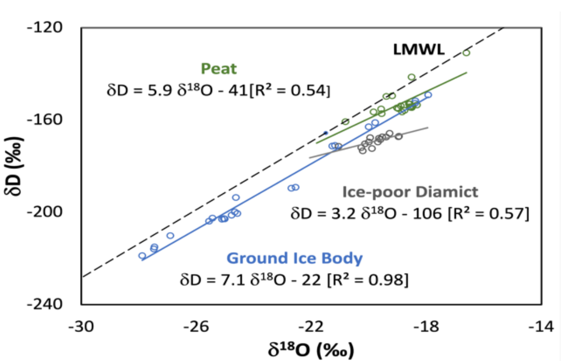

Figure 4. Co-isotope diagram of the three deposits in the NTGS17-01 borehole, along with the LMWL (s = 7.4).

4.3 Unit 3: Upper Layered Unit

This upper layered unit (2.3 to 2.7 m) displays a tabular appearance (i.e., flat, sheet-like appearance) with alternating translucent and opaque ice layers (Figure 3a). This tabular ice unit has layered cryostructures, with translucent layers varying in thickness between 0.5 and 1.5 cm. The CT scan statistics show similar statistics to unit 5 (lower layered unit) between the opaque and translucent layers (Table 1).

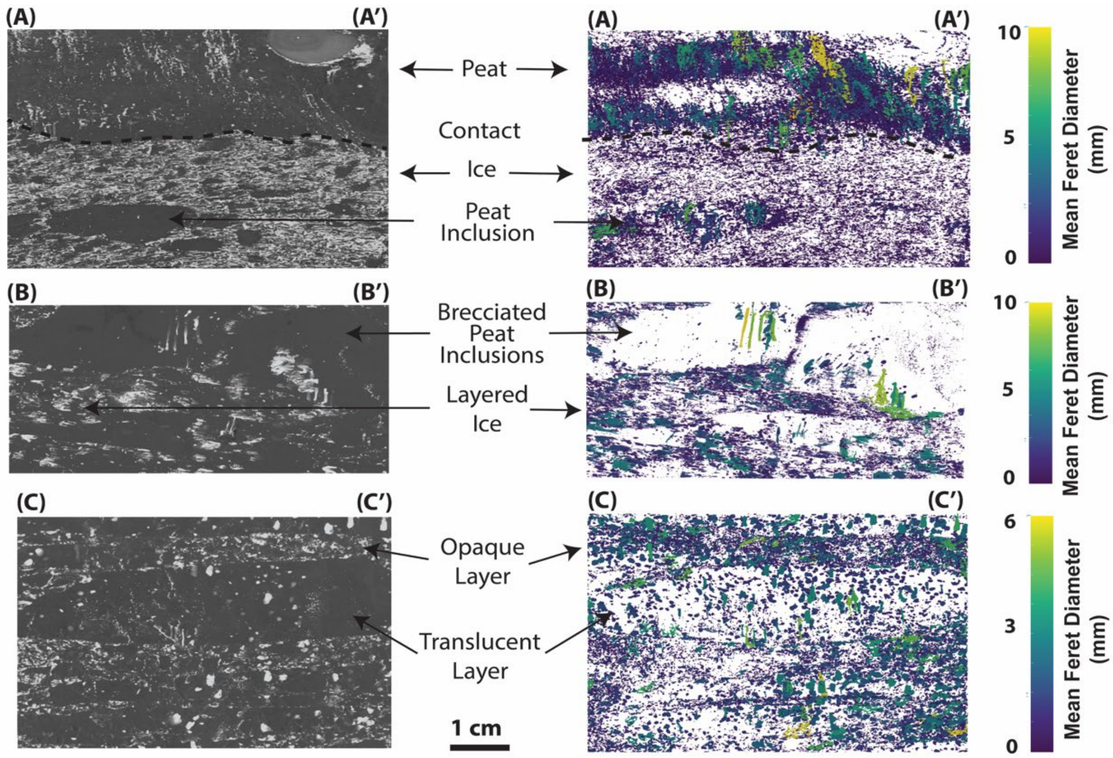

Figure 5. CT scans of the ice body with stratigraphic positions are indicated in Figure 3. The left figures show gas bubbles in white relative to ice and peat in black, while the right figures show the mean Feret diameter and orientations of gas bubbles, for the same field of view at the left figures. (A) Contact unit. High concentration of very small bubbles below the contact and long tubular bubbles above the contact and within peat inclusions (B) Brecciated unit. Bimodal distribution of bubbles with long tubular bubbles within peat inclusions and small bubbles within the layered ice. (C) Layered unit showing bimodal distribution of bubbles with upwards-tapering elongated bubbles within translucent layers and a high concentration of small bubbles in the opaque layer.

4.4 Unit 4: Brecciated Unit

The brecciated unit (2.7 to 3.5 m) has milky-white ice with brecciated (angular) organic inclusions (Figure 3b). This sediment-poor ice unit has lenticular, layered and suspended cryostructures. The organic inclusions vary in size, with larger inclusions between 1 and 3 cm thick and 7–10 cm wide (larger inclusions were as wide as the 10 cm diameter core). These angular organic inclusions are fractured but occur roughly parallel to the underlying layered ice unit. Gas bubbles within the peat inclusions vary between small spherical bubbles and long tubular bubbles, with a maximum Feret diameter of 9 mm.

These long tubular bubbles thin downwards and occur normal to the base of the angular inclusions, consistent with the overlying peat unit (Figure 5B). There is a bimodal distribution of bubbles within this unit, with gas bubbles within the peat inclusions having an average gas bubble concentration of 1%, despite being ~200% larger than bubbles in the sediment-poor layered ice (Figure 5B). The gas bubbles within the peat inclusions have a mean Feret diameter of 0.46 mm, a mean volume of 0.06 mm^3, and a mean sphericity of 0.88. The gas bubbles concentration within the ground ice layers is 11%. The gas bubbles within the layered ice have a mean Feret diameter of 0.34 mm, a mean volume of 0.03 mm^3, and a mean sphericity of 0.87.

4.5 Unit 5: Lower Layered Unit

The lower layered unit (3.5 m to 6.9 m) has a tabular appearance with alternating layers of translucent and opaque ice (Figure 3c,d). The translucent ice layers, or lenses, vary in thickness between 0.5 and 2 cm, with a low concentration of bubbles (average gas bubble concentration 4%). Some translucent layers show upward-tapering bubble trains, elongated bubbles, and vertical tubular bubbles (Figure 5C). Gas bubbles within the translucent layers have a mean Feret diameter of 0.52 mm, mean volume of 0.07 mm^3, and a mean sphericity of 0.85. The opaque, milky-white layers vary in thickness between 0.1 and 0.6 cm, with a greater concentration of fine bubbles (average gas bubble concentration of 11%) and no bubble trains. Gas bubbles within the opaque layers have a mean Feret diameter of 0.27 mm, mean volume of 0.01 mm^3, and mean sphericity of 0.90. The opaque layers tend to host a higher concentration of smaller bubbles with higher sphericity (Figure 6; Table 1). This contrast between translucent and opaque layers leads to a banded appearance, overall. In total, between units 3 and unit 5 there are a total of ~120 banded-pair layers. Additionally, for this layered unit we a tested the isotopic signatures of a few core segments at a higher resolution between the layers (Figure 6). Overall, the translucent layers have a slight δ^{18}O depletion (~-0.2‰) relative to the opaque layers.

4.6 Unit 6: Ice-poor Diamict Unit

An ice-poor diamict unit is present from 6.9 m to the base of the borehole at 11.2 m (Figure 3e). This unit has a sharp contact with the overlying ground ice deposit. This unit is mostly ice-poor with rare lenticular and vein cryostructures varying in thickness between 1 and 5 cm.

5 Interpretation and Discussion

Several cryostratigraphic and isotopic features of the NTGS17-01 ground ice body, peat, and diamict deposits preclude common ground ice types in the region. First, this body of ice, 2.1 m below the ground surface, and about 1.3 m below the permafrost table, comprises relatively pure ice, without significant mineral inclusions. This suggests that it's not aggradational ice of segregated origin (i.e., a rising permafrost table in the near surface) due to the absence of near-surface mineral soil with many small (mm to cm thick), segregated lenses (Kokelj and Burn 2003). As it is a peatland that lacks any significant slope, and there's an absence of mass wasting or alluvial sediments in the core, the possibility of a rapid burial mechanism for surface ice preservation (i.e., aufeis, lake ice, or snowbank) is unlikely. Another common ice type within peatlands is wedge ice, but negative d-excess values and the absence of vertical foliations preclude a wedge ice origin. Lastly, this ice type does not exhibit the typical characteristics of segregated ice, which include massive appearance, i.e., homogenous without structure, translucent without mineral inclusions, and gradational contacts with adjacent material (Mackay 1989; Pollard 1990; French and Harry 1990). Buried glacier ice is a common feature in permafrost-preserved Pleistocene till deposits of the Laurentide Ice Sheet (French and Harry 1990; Murton et al. 2005; Kokelj et al. 2017) and locally, in the moraine demarcating the Sitidgi Stade ice limit (Rampton 1988). In addition, large, tabular segregated-intrusive ice bodies, interpreted to be of Laurentide Ice sheet meltwater origin have been described for areas of the Tuktoyaktuk Coastlands by Dallimore and Wolfe (1988) and Mackay and Dallimore (1992). However, these ice bodies are typically underlain by sandy deposits, and often associated with positive relief known as involuted hills (Dallimore and Wolfe 1988). However, the relatively high isotopic values of the ice body and the lower diamict, rule out its origin as a buried glacier or segregated ice of glacier-meltwater origin. The average δ^{18}O value is -23.5‰, which is enriched relative to Pleistocene values in the region and most similar to Holocene waters with minor evaporative enrichment (e.g., Lacelle et al. 2004). The regression line with a slope of 7.1, similar to the LMWL, suggests a meteoric water source (Figure 4). Further, δ^{18}O values, range from –-27‰ to -18‰, suggest the ice layers capture seasonal variations in precipitation and coupled with the age of the basal peat and the presence of peat inclusions, indicate the ice body formed during the late Holocene.

Another possibility is that the thick ice body is of pool ice origin (also sometimes termed thermokarst cave ice), which can be found within ice-wedge polygon networks (Mackay 1988, 1997). Pool ice can have a banded structure similar to injection ice (Mackay 1988). However, the ground ice body in NTGS17-01 lacks common pool ice characteristics of reticulate-chaotic cryostructures at sediment contacts (Fortier et al. 2008) or radial bubble train dispersion from lateral freezing processes (Mackay 1997; Kotler and Burn 2000). Despite this, some 'injection ice' can form if water within the ice-wedge troughs is pushed or "injected" into the active layer of adjacent polygon ridges by cryostatic pressure (Mackay 2000). This type of ice developed by injection processes has been observed in poorly drained ice-wedge terrain similar to this study site by Mackay (2000), who refers to it as a type of 'pool ice'.

We interpret the 4.8-m-thick NTGS17-01 ground ice body as injection ice based on several lines of evidence. First, the stratigraphy of the ground ice body displays distinct sharp horizontal contacts that are concordant with the diamict and peat deposits. Where a concordant ice body is an ice body that is aligned parallel to host deposits. The water is likely injected at the interface between the frozen peat and underlying mineral soil. Van der Sluijs et al. (2018) describe a similar scenario, with injection ice occurring between the

Table 1. Summary of gas inclusions (bubbles) characteristic for all the ice deposit units, including sphericity, Feret diameter, volume, and gas bubble concentration (volume of gas over the total volume) with standard deviations (SD).

Peat Unit & Inclusions	**Mean Feret Diameter** [± SD] **(mm)**	**Mean Volume** [± SD] **(mm³)**	**Mean Sphericity** [± SD]	**Gas Bubble Concentration (%)**
Unit 1: Peat	0.56 ± 0.54	0.05 ± 0.17	0.81 ± 0.15	5
Unit 2 (Contact) Peat Inclusions	0.49 ± 0.46	0.03 ± 0.08	0.85 ± 0.14	9
Unit 4 (Brecciated) Peat Inclusions	0.46 ± 0.83	0.06 ± 0.24	0.88 ± 0.14	1
Ground Ice Units	**Mean Feret Diameter** [± SD] **(mm)**	**Mean Volume** [± SD] **(mm³)**	**Mean Sphericity** [± SD]	**Gas Bubble Concentration (%)**
Unit 2: Contact	0.33 ± 0.24	0.01 ± 0.03	0.88 ± 0.11	21
Unit 4: Brecciated	0.34 ± 0.32	0.03 ± 0.09	0.87 ± 0.14	11
Unit 3/5: Layered: Translucent Layers	0.52 ± 0.41	0.07 ± 0.21	0.85 ± 0.14	4
Unit 3/5: Layered: Opaque Layers	0.27 ± 0.25	0.01 ± 0.06	0.90 ± 0.12	11

uplifted peat and mineral soil interface. Whereby, water flow is impeded by physical obstacles (including road embankments and frozen culverts) or frozen soil, it results in hydrostatic and cryostatic pressure. This, in turn, causes the injection of ice, and the upwards displacement of the overlying frozen material (van der Sluijs et al. 2018). Moreover, this concordant interpretation is further highlighted in the bubble size and orientation at the contact between the ground ice and peat deposits. The contact unit (depth 2.1 to 2.3 m) features opaque, milky-white ice characterized by a high gas bubble concentration of 11% and small air bubbles (mean Feret diameter and volume of 0.33 mm and 0.01 mm^3, respectively). While the peat unit shows long downward-tapering bubble trails towards the contact. We interpret the ice at the contact between unit 1 and unit 2, as having frozen rapidly with a downward freezing front. The small bubbles in the contact unit are likely caused by a chill zone by the overlying frozen peat deposit, similar to Pollard (1990), which would reflect rapid downward freezing of pressurized water.

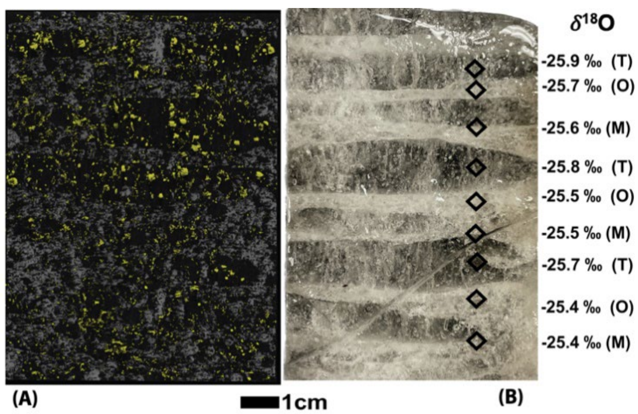

Figure 6. Layered unit with the stratigraphic position indicated in Figure 3d. (A) CT scan showing ice in black relative to small gas bubbles (white) and large elongated bubbles (yellow) with a mean Feret diameter of 0.27mm and 0.52mm, respectively. (B) Photo of layered ice with high resolution isotope sampling between translucent (T), opaque (O) and mixed (M) layers.

Second, the water isotope record highlights at least some seasonal variation, with $\delta^{18}O$ ranging from -17.9‰ to -27.9‰, indicative of modern summer and winter/spring precipitation (Fritz et al. 2022). Water that makes up injection ice bodies should comprise late-season precipitation with perhaps some snowmelt. Moreover, the co-isotope slope of the ice body is 7.1, similar to the LMWL. In contrast, the co-isotope slope of the peat deposit and ice-poor till are 5.9 and 3.2, respectively (Figure 4). These data are consistent with water sourced from an open reservoir, suggesting an accumulation of the ice body and surface heave within winter months, rather than segregation from the overlying or underlying deposits.

Third, the most common cryostructures within the ground ice body are layered, underlining the horizontal tabular form within units 2 and 4. This layered appearance is governed by bubble sphericity, bubble size and gas bubble concentration. Within these units, there are alternating layers highlighting a banded nature to the ice with distinct cryotextures. Thinner, opaque layers contain smaller, spherical bubbles (mean Feret diameter of 0.27 mm) and a gas bubble concentration of 11%, while translucent layers have larger elongated and upward-tapering bubbles (mean Feret diameter of 0.52 mm), aligned parallel to freezing directions. This banded appearance with elongated bubbles parallel to the freezing direction is similar to injection ice reported by Mackay (1972, 1990, 1998), and Pollard and French (1985), and it is attributed to multiple generations of injection ice whereby upward tapering bubbles align in the direction of heat flow. In addition, the opaque and translucent layers display differing bubble concentrations. We interpret the layering as first-ice and last-ice processes. This process is based on the notion that the initial ice tends to be clear, as it expels dissolved solutes, thereby reducing impurities and gas bubbles. This succeeded by the freezing of the remaining water containing a higher concentration of gases and impurities. First-ice and last-ice processes has been observed by Mackay (1990), within a seasonal time frame, whereby he suggests that clear ice bands with large gas bubble trails represent fast freezing ice in winter months, meanwhile the opaque, gas-rich bands represent slow freezing ice in summer months. These forms are similar to the banded ice described by Mackay (1988, 1990) in pingos, and Pollard and French (1985) in frost blisters, whereby the layering is governed by multiple generations of seasonal first-ice and last-ice processes. However, the isotopic differences within the layers of the ice body in NTGS17-01 do not align with first-ice and last-ice processes at seasonal timescales (Figure 6B). Instead, we interpret this banding as a first-ice and last-ice process within a rapid freezing environment. Therefore, we interpret that the translucent layers freeze first and have a lower bubble concentration (4% gas bubble concentration) leading to their greater light penetration. In contrast, the last-ice formation typically consists of opaque, bubble-rich layers (11% gas bubble concentration).

Lastly, this ice deposit has peat inclusions within the contact and brecciated units. These peat inclusions feature long (up to 9 mm) tubular bubbles that narrow downwards. Brecciated inclusions have also been observed in some segregated ice bodies (Shumskii 1964; Pollard 1990). However, the long downward-tapering bubbles within the peat inclusions contrast bubble trends throughout the ice deposit, including upward-tapering bubbles in some of the translucent layers of unit 4 or the absence of bubble trails within the other ice units. Therefore, the downward-tampering bubbles, which go against the direction of heat flow within the ice, suggest a downward displacement of fragmented frozen peat, brittle deformation, from the overlying peat deposit. This displacement is likely a result of pressurized water lifting the frozen peat and integrating brecciated fragments prior to freezing (Figure 7).

5.1 Layered Intrusive Ice Conceptual Model

Given the available evidence, the likely origin of the ground ice body is as intrusive ground ice. Our hypothesis is that the injected water originates from meteoric sources based on the isotope data. This injected water likely comes from a combination of two meteoric sources: (1) pond water within ice-wedge troughs, which if truncated by thaw can exceed 2 m depth relative to the surface of the adjacent polygon centers, and (2) a riparian zone located ~10 m uphill, whereby a constant water source routed through an ice-wedge trough network provides a hydraulic head. These two water sources allow for hydraulic pressure coupled with last-to-freeze pond water sitting adjacent to the peat-diamict interface (Figure 7). Similar forms of injection ice, governed by cryostatic pressures, have been observed by Mackay (2000) in ice-wedge polygons, adjacent to stream banks (Kane 1981), and due to road embankments and blocked culverts along the Dempster (van der Sluijs et al. 2018) and Inuvik-Tuktoyaktuk Highway. Cryostatic pressure can build in pockets of unfrozen material between the downward-freezing active layer and the permafrost table, typically during the winter freeze-back (Mackay and Mackay 1976). The rhythmic alternation between the bubble-rich opaque and translucent ice is interpreted to record multiple episodes of water injection, perhaps within a single year. Notably, the thickness of band-pairs (translucent and opaque layers) in the ice body ranges from ~3 cm to 5 cm

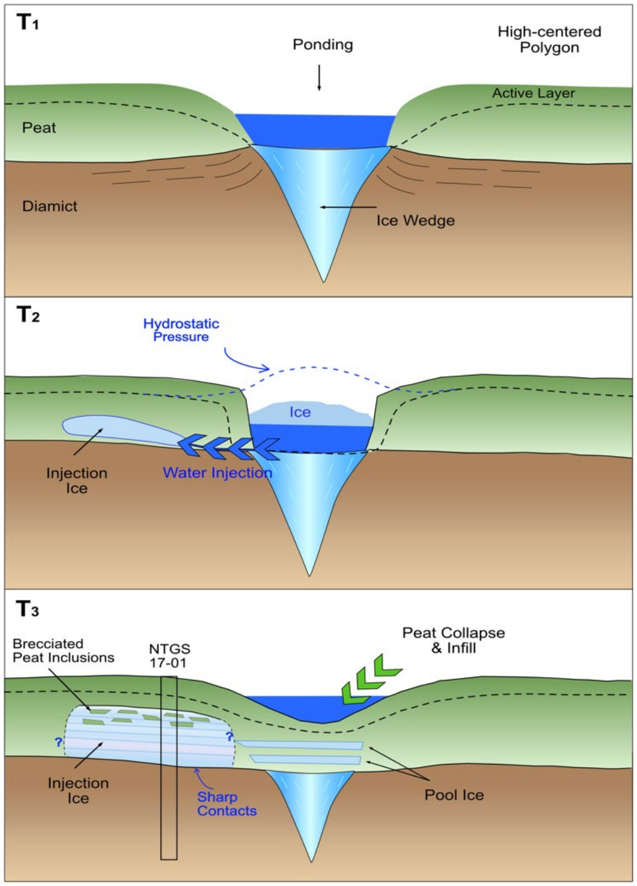

Figure 7. Conceptual model of layered intrusive ice formation in a high-centered ice-wedge polygon, based on Kane (1981) and Mackay (2000). (T1) Active layer expansion and ponding in ice wedge. (T2) Development of injection ice lens from hydrostatic head due along the peat and diamict contact. (T3) Growth of banded ice body from repeated injection events. Resulting uplift causes peat infilling troughs coincident with pool ice formation.

which differs significantly from the band-pairs in pingo ice (10 to 60 cm). This variation is noteworthy because Mackay (1990) interprets each pingo band-pair to represent 1 year of growth, with the translucent layers indicating fast-freezing winter injections, while opaque layers are interpreted as slower-freezing summer injections. In contrast, the NTGS17-01 intrusive body likely does not conform to this yearly seasonal pattern within the bands; rather, we suggest these ~120 band pairs may correspond to distinct ice growth pulses. It is challenging to determine the exact number of years it took to form the banding; however, the isotopic evidence coupled with freezing cryostatic pressure suggests that these periods of growth primarily occur during the winter season.

6 CONCLUSIONS

This study assesses the origin of an anomalously thick layered ice body at the interface between the peat and underlying diamict in a 11.2 m peatland core adjacent to the ITH highway. We interpret the 4.8-m-thick ground ice body as concordant intrusive ice based on: (1) sharp contacts and a chill zone within the upper contact with the overlying peat; (2) winter isotopic signature with a co-isotope slope suggestive of open-source water; (3) tabular appearance with distinct band-pair layering indicative of first-ice and last-ice processes; and (4) peat inclusions within the ice, indicative of pressurized frozen peat displacement. This intrusive ice is, therefore, likely formed by hydrostatic pressure in ice-wedge troughs (where water tends to freeze last), forcing water under pressure laterally into permafrost at the interface between the peat and the ice-poor diamict. This observation provides additional evidence that tabular ice bodies may comprise and important but underappreciated ice type in polygonal peatlands.

7 ACKNOWLEDGEMENTS

We gratefully acknowledge the Inuvialuit, whose land (Inuvialuit Settlement Region) this borehole was drilled on and material was retrieved from. This work has been supported by the Natural Sciences and Engineering Research Council (NSERC), UAlberta North, and Indigenous partners, including the Inuvialuit Land Administration. Additionally, we acknowledge the Government of Northwest Territories – Department of Infrastructure, the Aurora Research Institute, for their support of the Sentinel Drilling Program.

8 REFERENCES

Dallimore, S.R. and Wolfe, S.A. 1988. 'Massive ground ice associated with glaciofluvial sediments, Richards Island, N.W.T. Canada', in K. Senneset (ed.), *Fifth International Conference on Permafrost*, Trondheim, Norway, volume 1, pp. 132–136.

Ensom, T., Morse, P.D., Kokelj, S.V., MacDonald, E., Young, J., Tank, S., Subedi, R., Grozic, E. and Castagner, A. 2020. 'Permafrost geotechnical borehole data synthesis: 2013–2017 Inuvik-Tuktoyaktuk region', *Northwest Territories Geological Survey* NWT Open Report 2019-012 (also Geological Survey of Canada Open File 8652). doi:10.4095/321869.

Fortier, D., Kanevskiy, M., and Shur, Y. 2008. 'Genesis of Reticulate-Chaotic Cryostructure' in *Permafrost, Proceedings of the Ninth International Conference on Permafrost*, Fairbanks, Alaska, United States, volume 1, pp. 451–456. doi:10.13140/2.1.4703.3929.

French, H.M. and Harry, D.G. 1990. 'Observations on buried glacier ice and massive segregated ice, western arctic coast, Canada', *Permafrost and Periglacial Processes* 1, pp. 31–43, doi:10.1002/ppp.3430010105.

Fritz, M., Wetterich, S., Mcalister, J., and Meyer, H. 2022. 'A new local meteoric water line for Inuvik (NT, Canada)', *Earth System Science Data* 14**,** pp. 57–63. doi:10.5194/essd-14-57-2022.

Kane, D.L. 1981. 'Physical mechanics of aufeis growth', *Canadian Journal of Civil Engineering* 8, pp. 186–195. doi:10.1139/l81-026.

Kennedy, K.E., Froese, D.G., Zazula, G.D., and Lauriol, B. 2010. 'Last Glacial Maximum age for the northwest Laurentide maximum from the Eagle River spillway and delta complex, northern Yukon', *Quaternary Science Reviews* 29, pp. 1288–1300. doi:10.1016/j.quascirev.2010.02.015.

Kokelj, S. V. and Burn, C.R. 2003. 'Ground ice and soluble cations in near-surface permafrost, Inuvik, Northwest Territories, Canada', *Permafrost and Periglacial Processes* 14, pp. 275–289, doi:10.1002/ppp.458.

Kokelj, S.V., Palmer, M.J., Lantz, T.C., and Burn, C.R. 2017. 'Ground Temperatures and Permafrost Warming from Forest to Tundra, Tuktoyaktuk Coastlands and Anderson Plain, NWT, Canada', *Permafrost and Periglacial Processes* 28, pp. 543–551, doi:10.1002/PPP.1934.

Kotler, E. and Burn, C.R. 2000. 'Cryostratigraphy of the Klondike "muck" deposits, west-central Yukon Territory', *Canadian Journal of Earth Sciences* 37, pp. 849-861, doi:10.1139/e00-013.

Lacelle, D., Bjornson, J., Lauriol, B., Clark, I.D., and Troutet, Y. 2004. 'Segregated-intrusive ice of subglacial meltwater origin in retrogressive thaw flow headwalls, Richardson Mountains, NWT, Canada', *Quaternary Science Reviews* 23, pp. 681–696. doi:10.1016/j.quascirev.2003.09.005.

Mackay, J.R. 1972. 'The World of Underground Ice', *Annals of the Association of American Geographers* 62, pp. 1–22. doi:10.1111/j.1467-8306.1972.tb00839.x.

Mackay, J.R. 1988. 'Catastrophic lake drainage, Tuktoyaktuk Peninsula area, District of Mackenzie'**,** *Geological Survey of Canada* Paper 83-1D, pp. 83–90. doi:10.4095/122663.

Mackay, J.R. 1989. 'Massive ice: some field criteria for the identification of ice types', *Geological Survey of Canada* Paper 89-1G, pp. 5–11.

Mackay, J.R. 1990. 'Seasonal growth bands in pingo ice', *Canadian Journal of Earth Sciences* 27, pp. 1115–1125. doi:10.1139/e90-116.

Mackay, J.R. 1997. 'A full-scale field experiment (I 978 - I 995) on the growth of permafrost by means of lake drainage, western Arctic coast: a discussion of the method and some results', *Canadian Journal of Earth Sciences* 34, pp. 17–33. doi.org/10.1139/e17-002.

Mackay, J.R. 1998. 'Pingo growth and collapse, Tuktoyaktuk Peninsula area, western arctic coast, Canada: A long-term field study', *Geographie Physique et Quaternaire* 52, pp. 271–323. doi:10.7202/004847ar.

Mackay, J.R. 2000. 'Thermally induced movements in ice-wedge polygons, western arctic coast: A long-term study', *Geographie Physique et Quaternaire* 54, pp. 41–68. doi:10.7202/004846ar.

Mackay, J.R. and MacKay, D.K. 1976. 'Cryostatic pressures in nonsorted circles (mud hummocks), Inuvik, Northwest Territories', *Canadian Journal of Earth Sciences* 13, pp. 889–897.

Mackay, J.R. and Dallimore, S.R. 1992. 'Massive ice of the Tuktoyaktuk area, western Arctic coast, Canada', *Canadian Journal of Earth Sciences* 29, pp. 1235–1249. doi:10.1139/e92-099.

Morse, P.D. and Burn, C.R. 2014. 'Perennial frost blisters of the outer Mackenzie Delta, western Arctic coast, Canada', *Earth Surface Processes and Landforms* 39, pp. 200–213. doi:10.1002/esp.3439.

Murton, J.B. and French, H.M. 1994. 'Cryostructures in permafrost, Tuktoyaktuk coastlands, western Arctic Canada', *Canadian Journal of Earth Sciences* 31, pp. 737–747. doi:10.1139/e94-067.

Murton, J.B., Whiteman, C.A., Waller, R.I., Pollard, W.H., Clark, I.D. and Dallimore, S.R. 2005. 'Basal ice facies and supraglacial melt-out till of the Laurentide Ice Sheet, Tuktoyaktuk Coastlands, western Arctic Canada', *Quaternary Science Reviews* 24, pp. 681–708

Pollard, W. 1990. 'The nature and origin of ground ice in the Herschel Island area, Yukon Territory', in M. Burgess, D. Harry, and D. Sego (eds.), Proceedings of the fifth Canadian Conference on Permafrost, Québec City, Québec, pp. 23–30. Available at: http://pubs.aina.ucalgary.ca/cpc/cpc5-23.pdf.

Pollard, W.H. and French, H.M. 1985. 'The Internal Structure and Ice Crystallography of Seasonal Frost Mounds', *Journal of Glaciology* 31, pp. 157–162. doi:10.3189/s0022143000006407.

Rampton, V.N. 1988. 'Quaternary Geology of the Tuktoyaktuk Coastlands, Northwest Territories', *Geological Survey of Canada* Memoir 423. Available at: https://doi.org/10.4095/126937.

Reyes, A. V, Jensen, B.J.L., Zazula, G.D., Ager, T.A., Kuzmina, S., La Farge, C., and Froese, D.G. 2010. 'A late-Middle Pleistocene (Marine Isotope Stage 6) vegetated surface buried by Old Crow tephra at the Palisades, interior Alaska', *Quaternary Science Reviews* 29, pp. 801–811. doi:10.1016/j.quascirev.2009.12.003.

Roustaei, M., Pumple, J., Harvey, J., and Froese, D. 2022. 'Estimating ice and unfrozen water in permafrost samples using industrial computed tomography scanning', in *GeoCalgary 2022*. Calgary, Alberta, Canada.

Rudy, A.C.A., Kokelj, S.V., Morse, P.D., and Ensom, T. 2020. 'Permafrost Ground Temperature Report: Inuvik to Tuktoyaktuk Highway Sentinel sites', *Northwest Territories Geological Survey* NWT Open Report 2019-017. Available at: https://doi.org/10.46887/2019-017.

Shumskii, P.A. 1964. 'Ground (subsurface) ice', *National Research Council of Canada* Technical Translation. doi.org/10.4224/20386780.

van der Sluijs, J., Kokelj, S.V., Fraser, R.H., Tunnicliffe, J., and Lacelle, D. 2018. 'Permafrost terrain dynamics and infrastructure impacts revealed by UAV photogrammetry and thermal imaging', *Remote Sensing* 10, 1734. doi:10.3390/rs10111734.